Porous Flow and Sediment Transport Simulation for Physically-Based Weathering

Theo Jonchier, Arthur Cavalier, Thibault Tricard, Guillaume Gilet, Stephane Merillou

Volume xx (200y), Number z, pp. 1–13

Porous Flow and Sediment Transport Simulation for Physically-Based Weathering

T. Jonchier[1], A. Cavalier[2], T. Tricard[3], G. Gilet[4] and S. Merillou[1]

[1]Université de Limoges, XLIM, CNRS, UMR 7252, Limoges, F-87000, France
[2]Université de Poitiers, XLIM, CNRS, UMR 7252, Poitiers, F-86000, France
[3]Université de Lorraine, CNRS, INRIA, LORIA, Nancy, F-54000, France
[4]University of Sherbooke, Department of Computer Science, Sherbrooke, Canada

Figure 1: *Coffee is dissolved in the water that gets inside the filter. Concentrated water then seeps through the filter to reach the glass. From left to right: Render of the scene, solid and wetting, fluid and its contained sediments, sediments density.*

Abstract

In the graphic community, rendering lifelike scenes remains an open challenge. Among the features required to reach photorealism, aging is the crucial detail that breaks the pristine aspect that is rarely observed in real life. Multiple approaches have been proposed, from example-based to physical simulation, to compute the aging of an object. In this context, we present a simulation framework that handles multiple weathering effects causing an object to alter over time. We identify the key phenomena (wetting, drying, erosion, deposition, and dissolution) and propose a base framework to address the aging process. To tackle this challenge, our method adapts a Smooth Particle Hydrodynamics model to represent external fluids (i.e., classical fluid simulation) and internal porous flow. Our framework handles the wetting, drying, and flow in the porous space in a unified approach. We extend pre-existing sediment transport method to allow the sediment transport outside and inside the porous space. With our method, sediments can be eroded from a solid surface, transported across solid objects through their porous space, and deposited to modify other objects' properties across the scene.

1. Introduction

As stated by Becket and Badler [BB90], an ideal renderer cannot produce realistic imagery if the virtual scene only exhibits pristine objects. In real life, appearances of objects are constantly modified by their surrounding environment. Those modifications can be reversible (wetting, dust deposition, deformations, etc.) or definitive (cracks, scratches, rust, etc.). Aging can impact many of the properties of the objects (geometric, chemical, optical, mechanical) and should always be considered when rendering a photorealistic scene. Usually, geometries and/or textures are authored manually to emulate those appearances modifications. However, dealing with the complexity and the number of underlying phenomena is a time-consuming and challenging task, leading to heavy manual authoring requiring advanced physical knowledge.

Dorsey et al. [DRS07] classified the processes affecting appearance in three categories: mechanical, chemical, and biological. As each process can affect several properties of the material, Merillou and Ghazanfarpour [MG08] classified them with a phenomenolog-

ical approach. In the same way, we identified that most appearance changes are due to the simultaneous interactions between elementary phenomena. Based on previous works, we highlight a set of phenomena that are key to tackling the aging problem:

Deposition: Deposition is a process where a deposit of matter is left behind after the interaction between a surface and a fluid carrying micro-particles. Deposits cover the initial surface and affect the object's albedo, geometry, and physical properties. They can accumulate to create durable volumes of matter or be cleaned off by further fluid interactions. See **A** in Fig. 2.

Dissolution: When an object interacts with a fluid, part of the matter can pass into the fluid phase. This reaction affects geometry and the albedo/light absorption of the solvent. See **B** in Fig. 2.

Erosion: Erosion is a generic concept where fluid interactions alter the surface. It can be a direct consequence of dissolution or mechanical interactions between the object and the fluid. In this article, we consider erosion as a mechanical phenomenon. See **C** in Fig. 2.

Chemical reaction: A chemical reaction occurs when reactants interact to form new products. When fluids and/or solids get in contact their chemical compositions are altered, thus modifying their physical properties, albedo, and geometry. See **D** in Fig. 2.

Organic growth: Fluids transport seeds or spores. Those can take root object surfaces or within the porous space. External factors may activate plant growth (temperature, moisture, illumination). In addition, roots create internal stress, which deforms the host object and creates new geometry. See **E** in Fig. 2.

Deformation, cracks and peeling: When a material undergoes regular environmental changes such as variations in temperature or moisture level, its properties can be altered. Depending on the material, the frequency, and the magnitude of these changes, deformations may occur and create cracks or peelings in the case of thin layers. See **F** in Fig. 2.

Impacts and scratches: Mechanical interactions between objects can introduce surface alteration at different scales. Both microscopic scratches and collision-induced impacts change the surface geometry. More pernicious interactions can cause damage to a material's protective layer, thus allowing the intervention of other phenomena (e.g., impact on a car paint removing rust protection of the underlying metal). See **G** in Fig. 2.

All the previously described phenomena strongly correlate with the transport of matter both inside the objects (due to porosity) and on their surfaces. Moreover, they interact through this matter flow, making the aging process of very complex systems challenging to model accurately. Indeed, changing the behavior of any part of the process may impact the flow and change or even prevent any aging phenomenon from occurring.

In this paper, we propose to address these issues by introducing a framework that can handle both temporary phenomena (such as wetting and evaporation) and definitive flow-based phenomena which do not dissipate without leaving a trace. In summary, our main contributions are:

- A generic simulation framework that can handle multiple phenomena simultaneously such as wetting and evaporation of water, erosion and dissolution of a solid material leading to the creation, transport and deposition of micro-particles from the initial object;
- An authoring pipeline to simulate the aging process of a pristine scene to achieve a plausible, realistic weathered counterpart;

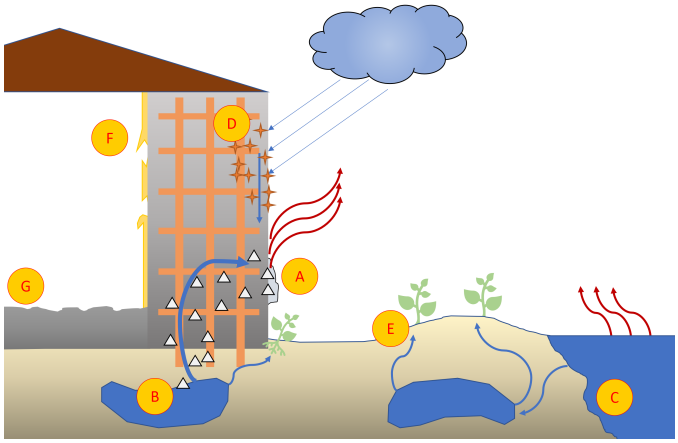

Figure 2: *Example scene featuring multiple weathering phenomena.* ***A****: Deposition or crystallization of salts at the building surface.* ***B****: Salt dissolution in the groundwater reservoir and its transport to the surface.* ***C****: River bed erosion.* ***D****: Corrosion of iron rods in armed concrete and transport of iron oxide to the surface through moisture.* ***E****: Organic growth favored by sun exposition and soil moisture level.* ***F****: Wall paints peeling due to humidity within the wall.* ***G****: Impacts and scratches on the floor.*

2. Previous Works

Reproducing realistic and complex weathered appearances is a challenging and trending task in computer graphics. As weathered appearances result from several concurrent physical phenomena, such a goal can be achieved either by the simulation of the underlying physical processes or through the direct synthesis of the final appearance using various input data guiding the synthesis.

Imaged Based Methods

Leveraging the inherent correlation between appearance and weathering phenomena, most of these methods compute a weathering degree map from appearance variations in input photographs or 3D scans. Explicit manipulation of the map provides artistic control over the result and allows for appearance transfer and arbitrary weathering or de-weathering of similar surfaces. The final appearance is then synthesized by reprojecting the corresponding visual content accordingly to the map.

By taking advantage of the non-uniformity of the weathered appearance of an otherwise uniform pristine object, an appearance manifold linking weathering phenomena and visual content can be built [WTL*06] to guide appearance synthesis. To absolve the method from heavy lighting restrictions in the capture process, Xu

et al. [XWT*08] propose to split the input photograph into reflectance and illumination component. The appearance manifold extracted from the input image is used to generate both the weathering degree and shading maps. After editing the weathering degree map, (de)weathered appearance can be synthesized by searching for the best candidate in the appearance manifold matching both weathering degree and lighting conditions. It also details how to transfer appearance between two pictures, successfully transforming corrosion present in a photo into organic growth extracted from another example.

Because appearance manifolds can be costly to construct, Bandeira and Walter [BW09] proposed to use an appearance map based on the Lab color space to alleviate the (de)weathered pixel color search. Bellini et al. [BKCO16] tackled the appearance synthesis of manufactured structures by exploiting the regularity of patterns found in those structures. Through the use of texture analysis, Lu, Dorsey, and Rushmeier [LDR09] extracted content-aware patches from input exemplars. Those are then distributed on a new texture to reproduce the input's spatial distribution and mesoscopic details.

By taking into account the correlation between local geometry and object appearance, a guidance map can be extracted from an input textured mesh [MKC*06,LGG*07]. Using this guidance map and a spatially varying texture synthesis model, the input mesh appearance can be mapped to another one. This automatic process removes the manual authoring of the weathering distribution map.

Physically Based Simulations

Several simulation-based approaches were proposed to accurately model and reproduce the weathering effect. The patina formation, for instance, can be simulated by combining the use of heightmaps and basic morphological operators to thicken or erode micro geometric surface details [DH96]. Following the idea of Dorsey et al. [DPH96], Chen et al. [CXW*05] proposed a generalized model of interaction between particles and surfaces that can represent multiple material property changes allowing stains, erosion, corrosion, and dirt deposition. While maintaining a good level of artistic control, this approach does not guarantee physically accurate results.

Dorsey et al. [DEJ*99] simulate the water flow that occurs in porous stones to tackle object aging. This approach lies on an eulerian simulation scheme computed in small cubic volumes aligned with the object surface called slabs. This method supports erosion, deposition, and sediments transport within and between the slabs. The underlying simulation data structures allow precomputing subsurface scattering. While this approach guarantees physically plausible results, it is limited to stones. In addition, the method requires a quad mesh representation to place voxels slabs correctly.

Estimating the fluid flow both inside and outside the materials pore space has been studied [LAD08]. Using Smooth Particle Hydrodynamics (later referred to as SPH), authors proposed a method supporting two-way coupling and elastic bodies to exhibit realistic wetting and deformations under pressure.

Wojtan et al. [WCMT07] proposed a method to compute animations of natural phenomena such as erosion, sedimentation, and acidic corrosion. Solids are represented using a level set stored in regular grids distinct from the grid used for fluid simulation. Level-set grids are then used to update the physical properties of solid objects.

Kristof et al. [KBKS09] use SPH to simulate hydraulic erosion, transport, and deposition of sediments on heightfield terrains. While limited to this representation, their approach produces realistic river beds and adds details to the terrain reliefs.

With both particle simulation and appearance manifold, Bosch et al. [BLR*11] proposed a hybrid approach. They combine extracted stains color and distribution information from a captured photograph [XWT*08] and a user-defined proxy mesh to produce a set of parameters driving a particle-based simulation capable of reproducing such appearance alterations. The particle simulation is then applied to novel virtual scenes.

Cracks and peeling on a planar surface can be estimated using [PPD02]'s method. By decomposing the surface into two layers, cracks and peeling are simulated using a 2D grid. A 3D mesh of the resulting peeled paint layer is then extracted. The process allows cracks to be user-defined via an input texture. However, this approach is limited to planar surfaces and does not take into account paint thickness.

Merillou et al. [MMGG12] investigated building degradations caused by salt decay. They proposed a model based on user-defined input textures to identify material's characteristics, such as albedo, porosity and salt concentration. By combining the procedurally computed crystallization depth and external atmospheric conditions, the model generates an aging-location texture. The latter is interpolated during rendering to alter material albedo or heightmaps.

Huber et al. [HPS11] proposed a liquid diffusion model in porous textiles based on SPH and a discrete cellular automaton to compute the various diffusion states. Interactions between hairs and water were also studied by Rungjiratananon et al. [RKN12]. They proposed using an eulerian grid to simulate the fluid diffusion within hairs where strands are modeled using connected lagrangian particles. Dripping is also taken into account when grid cells are oversaturated. Patkar et al. [PC13] proposed to model the wetting of porous solids by simulating liquid absorption, diffusion, and dripping on a tetrahedral mesh. While supporting mesh deformation and allowing two-way coupling between solids and fluids, advection is neglected.

Rungjiratananon et al. [RSKN08] proposed a model to tackle wetness propagation in granular materials. The latter is simulated using a combination of discrete element methods for granular materials and a SPH fluid simulation handling surface tension between granular particles. Mechanical interactions between granular materials and liquids have been recently studied and modeled using Material Point Methods by Gao et al. [GPH*18].

Recently, Munoz et al. [MPBM*18] proposed a method to model the pollution accumulation on building facades. Given a 2D map of the city and its pollution sources, such as traffic roads, a 2D Lattice-Boltzmann simulation is computed to obtain a wind map. This map is then used to compute a pollution map which stores the pollution propagation in the 2D scene. During rendering, they combine

screen-space techniques and material properties to estimate multiple factors which affect the final appearance such as insolation, pollution, porosity, wind accessibility, sky accessibility and rain accessibility.

As seen above, all these approaches commonly share the tendency to only tackle specific aging effects or to simulate a small number of them in a restricted context. However material appearance is not only affected by a specific phenomenon but by a conjoint intricated interaction of multiple weathering effects. In this paper, we propose a framework for the simulation of aging phenomena based on the computation of the fluid flow inside and outside the objects volume enabling the transport of sediments and solute through porous networks. It relies on Smoothed Particle Hydrodynamics which is a commonly used concept for solving numerical simulations of continuum mechanics. We refer the reader to an extensive state of the art of SPH-based methods [KBST19]. We present a comprehensive model handling: erosion, dissolution, deposition and evaporation as the combination of these phenomena are responsible for full changes in appearance.

3. Framework

Our model relies on a particle-based simulation using SPH continuum equations. As we want to correctly model interactions between fluids and solids, we distinguish two types of particles: fluid particles to model external fluid and solid particles to model inner fluid interactions through material pores, the latter embedding material-related fields such as porosity, permeability, capillary potential. All these particles p_i, centered at position $\mathbf{x_i}$, with a mass m_i, a density ρ_i (hence a volume $V_i = m_i/\rho_i$) are used to sample continuous properties (such as porosity, water saturation, temperature, etc.). Using the following SPH continuum equations, we can sample an arbitrary field A at an arbitrary position $\mathbf{x}$:

$$A(\mathbf{x}) \equiv \sum_j A_j V_j W(\mathbf{x_j} - \mathbf{x}) \tag{1}$$

$W(\mathbf{x_j} - \mathbf{x})$ being the standard cubic spline kernel defined as follow:

$$W(\mathbf{x_j} - \mathbf{x}) = \frac{8}{\pi h^3} \begin{cases} 6d^3 - 6d^2 - 1 & ,d \leq 0.5 \\ 2(1-d)^3 & ,0.5 < d < 1.0 \\ 0 & ,d \geq 1.0 \end{cases} \tag{2}$$

$$\text{with } d = \frac{||\mathbf{x_j} - \mathbf{x}||}{h} \tag{3}$$

In order to ease the notation, $W(\mathbf{x_j} - \mathbf{x_i})$ will be later referred as W_{ij}. Its gradient estimation sampled at particle p_i, noted ∇W_{ij}, is defined as follow:

$$\nabla W_{ij} = \frac{48}{\pi h^3} \frac{\mathbf{x_j} - \mathbf{x_i}}{||\mathbf{x_j} - \mathbf{x_i}|| h} \begin{cases} d(3d-2) & ,0 < d \leq 0.5 \\ (-1+d)(1-d) & ,0.5 < d < 1.0 \\ 0 & ,d \geq 1.0 \end{cases} \tag{4}$$

We can thus estimate the gradients and laplacian of a field A using equations (5) and (6) respectively.

$$\nabla A_{ij} \equiv \sum_j V_j A_{ij} \nabla W_{ij} \tag{5}$$

$$\nabla^2 A_{ij} \equiv \sum_j V_j A_{ij} \frac{2||\nabla W_{ij}||}{||\mathbf{x_j} - \mathbf{x_i}||} \tag{6}$$

We suppose the solid to be incompressible and thus can use $V_j = m_j/\rho_j$. However, if material compression is required, equations (1), (5) and (6) must use the mass-density ratio formulation.

In practice, our materials are defined by a set of properties such

Symbol	Description	Unit	Phase
i	Particle index	–	–
k	Material index	–	–
s_k	Sediment index	–	–
r	Particle radius	m	–
H	Relative humidity	–	–
$\mathbf{g}$	Gravity	$\mathrm{m \cdot s^{-2}}$	–
D^{s_k}	Sediment diffusivity	$\mathrm{m^2 \cdot s^{-1}}$	–
$\mathbf{x_i}$	Particle position	m	Both
V_i	Particle volume	$\mathrm{m^3}$	Both
V_i^f	Fluid volume	$\mathrm{m^3}$	Both
$V_i^{s_k}$	Sediment volume	$\mathrm{m^3}$	Both
$C_i^{s_k}$	Sediment concentration	–	Both
$\upsilon_i^{s_k}$	Sediment settlement velocity	$\mathrm{m \cdot s}$	Both
p_i^c	Capillary pressure	Pa	Both
T_i	Temperature	$\mathrm{C^\circ}$	Both
α_i	Heat diffusion coefficient	$\mathrm{m^2 \cdot s^{-1}}$	Both
S_i	Pores fluid saturation	–	Both
V_i^k	Material volume	$\mathrm{m^3}$	Solid
λ_i	Permeability	$\mathrm{m^2}$	Solid
β_i	Porous stiffness	Pa	Solid
σ^k	Material stress resistance	Pa	Solid
ϕ_i	Porosity	–	Solid
τ_i	Tortuosity	–	Solid
r^{s_k}	Sediment particle radius	mm	Solid
r^{p_k}	Caracteristic pore radius	mm	Solid
ρ_i	Density at particle i	$\mathrm{kg \cdot m^3}$	Fluid
ρ_0	Fluid rest density	$\mathrm{kg \cdot m^3}$	Fluid
μ	Dynamic viscosity	$\mathrm{Pa \cdot s}$	Fluid
	Control parameters		
κ_{concentr}	Concentration	–	–
κ_{depos}	Deposition	–	–
κ_{erosion}	Erosion	–	–
κ_{evap}	Evaporation	–	–
κ_{satur}	Saturation	–	–

Table 1: *Notation table. In the paper, per-particles properties are indexed using i and j. Properties linked to a material are exponentiated using k, those linked to a sediment of material k using s_k and the ones linked to the fluid using f. Control parameters permits to tune the simulation and to exacerbate specific effects as shown in the figures.*

as porosity, permeability, capillarity potential, temperature diffusivity, tortuosity (as seen in Table 1).

Each of our particles can aggregate several materials as needed. In such a case, their final properties are linearly interpolated according to the particle composition. This allows for the creation of complex materials as commonly found in nature (impurities in rocks or metal, for example) and reduces the number of particles needed to represent the scene. The global volume V_i can then be retrieved as the sum of the volume of each material of the solid particles.

Fluid particles represent both a volume of fluid and the volume of sediments they carry. As the maximal concentration of sediments in fluid particles remains low, its influence on volume variations can be safely neglected, simplifying the simulation.

We call "sediments" the set of properties describing the behavior of physical micro-particles contained in the fluid phase or trapped in the material pores. It can be used to represent both actual sediments (particles with a radius > micrometer) or soluble (particles with a radius < micrometer). Sediment is characterized by its density, diffusivity in water (solubility), the maximum concentration in water, and characteristic particle radius. Table 1 shows a compact version of all relevant data and their corresponding phases.

3.1. External Flow

As explained previously, we distinguish how particles behave depending on whether they are considered fluid or solid. Although we rely on an SPH fluid simulation to accurately model particles behavior, pressure acceleration, viscosity, surface tension, and boundary conditions must be carefully considered.

In practice, we rely on the pressure solver from [SP09, KBST19] to ensure incompressibility, namely preventing the fluid from constantly oscillating over time. Viscosity is considered fixed for the whole fluid using the standard model from [Mon05]. Surface tension is handled using [AAT13]'s approach. Finally, the volume field (i.e. $\sum_j V_j W_{ij} = 1$) is normalized to preserve boundary conditions, thus preventing fluid particles to get across solids.

3.2. Porous Flow

The key component of our method is to simulate the fluid flow in porous materials. Since our liquid particles can contain sediments, this step will then allow us to model the transport of sediments through the object and, thus, more generally, the transport of matter in the scene (see Section 3.3).

As described in [DEJ*99, LAD08], fluid flow traveling inside a porous medium is governed by Darcy's law [Dar56]. The latter (eq. (7)) expresses the instantaneous flux $\mathbf{q}$ of a fluid, with a dynamic viscosity μ and density ρ, traveling in a porous medium with a permeability λ, in relation with pressure gradient ∇p and gravity acceleration $\mathbf{g}$:

$$\mathbf{q} = -\frac{\lambda}{\mu}(\nabla p - \rho \mathbf{g}) \tag{7}$$

The fluid velocity within the medium (later referred to as porous velocity) can be retrieved by dividing the flux by the material porosity ϕ. While Darcy's law describes the porous flow for homogeneous mediums, it can be piecewisely adapted to simulate flow in heterogeneous mediums. As each solid particle is defined by its properties ϕ_i and λ_i, porous velocity can be rewritten using the SPH formalism to model the volume exchange within the medium. Porous velocity can thus be decomposed in two distinct parts: the diffusion velocity (Diff^f) and the advection velocity (Adv^f), respectively the rate at which a fluid will propagate from high to low-pressure locations and the rate at which gravity will guide the flow (see Fig. 3).

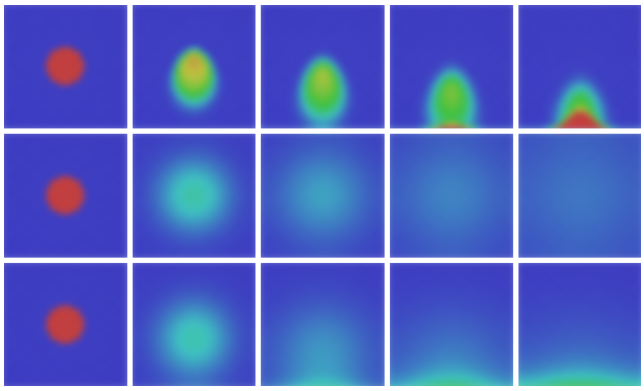

Figure 3: *A vertical slice of a solid homogeneous porous material saturated with water at its center (red disk). The heatmap shows the pore saturation in water (red is fully saturated and blue is dry).* ***first row:*** *Only the advection part is computed,* ***second row:*** *Diffusion part only,* ***third row:*** *Full computation of water flow within the porous medium*

$$\text{Diff}^f = -\frac{\lambda}{\mu\phi}(\nabla p) \tag{8}$$

$$\text{Adv}^f = -\frac{\lambda}{\mu\phi}(-\rho \mathbf{g}) \tag{9}$$

Diffusion: As stated by [LAD08], at the pore scale, the pressure applied on each particle is considered to be the capillary pressure p_i^c. Its differential will drive fluid from saturated pores to lesser ones:

$$p_i^c = \beta(1 - S_i)^{\kappa_{\text{satur}}} \tag{10}$$

Where β is the porous stiffness (or capillary potential) and $\kappa_{\text{satur}} \in [0;1]$ a constant controlling the influence of the saturation. The particle saturation S_i is defined as the ratio between the fluid volume V_i^f and the pore space $V_i\phi_i$ (i.e. the void volume of the particle):

$$S_i = \frac{V_i^f}{V_i \phi_i} \tag{11}$$

Since we consider the material is homogeneous and that we express the capillary pressure as a function of saturation, we can express equation (8) as a saturation diffusion process using the Muller

SPH diffusion formulation [MSKG05]:

$$\text{Diff}_i^f = -\sum_j \frac{\lambda}{\mu\phi}(p_i^c - p_j^c) V_j \nabla^2 W_{ij} \tag{12}$$

When multiple materials exist in a neighborhood, their particles exhibit different properties that cannot be interpolated directly without leading to incorrect behaviors. To prevent this, we must only consider the strongest constraints. We rewrite $\lambda/\mu\phi$ in a per-particle formulation:

$$\eta_i^p = \frac{\lambda}{\mu\phi} = \frac{\lambda_i}{\mu}\frac{1}{\phi_i} \tag{13}$$

Substituting (13) in (12) to account for the maximal resistance to fluid flow (smallest η^p) between particles i and j yields:

$$\text{Diff}_i^f = -\sum_j min(\eta_i^p, \eta_j^p)(p_i^c - p_j^c) V_j \nabla^2 W_{ij} \tag{14}$$

Since the diffusion is expressed as a function of the saturation, we need to transform it back to a flow rate.

$$\text{DiffV}_i^f = -V_i^f \sum_j min(\eta_i^p, \eta_j^p)(p_i^c - p_j^c) V_j \nabla^2 W_{ij} \tag{15}$$

Advection: To take into account fluid advection between porous solid particles, we chose to use a donor-acceptor scheme like the one proposed by Kristof et al. [KBKS09]. We identify an acceptor and a donor for each couple of particles i, j. Because we consider solid and fluid in the pore space as incompressible material, we assume that ρ is equivalent to its constant rest density ρ_0 in equation (9).

Similarly to the diffusion velocity, we must also take into account the maximal resistance to fluid flow using the minimal porous resistance between particles (using eq. (13)), thus we obtain:

$$\text{Adv}_i^f = -\sum_j \begin{cases} V_j min(\eta_i^p, \eta_j^p)(-\rho_0 \vec{g} \cdot \hat{\mathbf{x}_{ij}}) \|\nabla W_{ij}\| & , -\rho_0 \mathbf{g} \cdot \mathbf{x}_{ij} \geq 0 \\ V_i min(\eta_i^p, \eta_j^p)(-\rho_0 \vec{g} \cdot \hat{\mathbf{x}_{ij}}) \|\nabla W_{ij}\| & , -\rho_0 \mathbf{g} \cdot \mathbf{x}_{ij} < 0 \end{cases} \tag{16}$$

Where $\hat{\mathbf{x}_{ij}}$ denotes the normalized vector between particles i and j (i.e. $\frac{\mathbf{x_j} - \mathbf{x_i}}{||\mathbf{x_j} - \mathbf{x_i}||}$). Similary to equation (15), we transform the velocity to a flow rate and simplify the formulation:

$$\text{AdvV}_i^f = \sum_j \begin{cases} V_j^f V_j min(\eta_i^p, \eta_j^p) \rho_0 (\mathbf{g} \cdot \hat{\mathbf{x}_{ij}}) \|\nabla W_{ij}\| & , \mathbf{g} \cdot \mathbf{x}_{ij} \leq 0 \\ V_i^f V_i min(\eta_i^p, \eta_j^p) \rho_0 (\mathbf{g} \cdot \hat{\mathbf{x}_{ij}}) \|\nabla W_{ij}\| & , \mathbf{g} \cdot \mathbf{x}_{ij} > 0 \end{cases} \tag{17}$$

The final fluid volume variation at a given particle i is obtained by combining the diffusion and the advection part:

$$\frac{\partial V_i^f}{\partial t} = \text{DiffV}_i^f + \text{AdvV}_i^f \tag{18}$$

3.3. Sediment Transport

In a porous medium, sediments carried by fluid in the pore space get slowed down due to interaction with the pore's surface. As such, computing the water flow is not the only requirement to compute the sediment flow in such materials. Sediment transport in fluid, much like water movement in a porous medium, is affected by diffusion and advection components. The problem can thus be split as we previously did in Section 3.2.

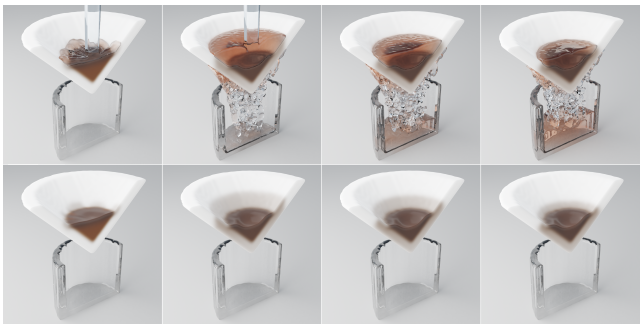

Figure 4: *Cut view illustrating dissolution of coffee passing through a porous medium following water flow.* ***Top row:*** *Render of water, solid, and sediment.* ***Bottom row:*** *Only solid surface is shown illustrating the dissolution process.*

Following [MSKG05], diffusion of an attribute A in a fluid in relation with its diffusion coefficient D can be expressed as follow:

$$\frac{\partial A}{\partial t} = D\nabla^2 A \tag{19}$$

In our case, the volume variation of sediments within the fluid combines the diffusion of the material sediments and the advection induced by the sediment settlement velocity. Given N the number of material present in the scene, we can compute the volume variation of a sediment s_k of a material $k \in [0, N]$ as the combination of the diffusive part (eq. (19)) and the sediment settlement velocity denoted υ^{s_k} :

$$\frac{\partial V_i^{s_k}}{\partial t} = D^{s_k} \nabla^2 C_i^{s_k} - \upsilon_i^{s_k} \tag{20}$$

Where V^{s_k} is the volume of sediment s_k, D^{s_k} is the diffusivity in water of the sediment s_k, and C^{s_k} correspond to the concentration of a sediment s_k :

$$C_i^{s_k} = \frac{V_i^{s_k}}{V_i^f + \sum_n^N V_i^{s_n}} \tag{21}$$

In addition, porous materials may exhibit complex internal pore geometry, referred to as tortuosity. The intrinsic pore geometry causes sediments to reduce their travel speed through the material. It limits the sediments' velocity within the pore space based on the ratio of the sediment characteristic radius r^{s_k} and the material's pore characteristic radius r^{p_k}. We represent tortuosity as an exponent τ which dictates how much r^{s_k}/r^{p_k} impacts sediment speed. A velocity reduction factor $filter$ can be expressed as:

$$\text{filter}_i = (1.0 - r^{s_k}/r_i^{p_k})^{\tau_i} \tag{22}$$

$$\text{filter}_{(i,j)} = \min(filter_i, filter_j) \tag{23}$$

Since the number of materials and sediment is finite for each

scene, a look-up table can be pre-computed for each couple sediment/material. Sediment diffusion (eq. (24)) is governed by a diffusivity factor D^{s_k} which represents how sediments would spread in its carrier (water in our case). We consider the filter parameter of the particle with the strongest constraint (eq. (23)) to avoid smoothing artifacts.

$$\mathrm{Diff}\mathrm{V}_i^{s_k} = V_i^f \sum_j \mathrm{filter}_{(i,j)} D^{s_k} (C_i^{s_k} - C_j^{s_k}) V_j^f \nabla^2 W_{ij} \tag{24}$$

Sediments may settle with time due to their density being heavier than water. Because of that, diffusion only is not enough to represent sediment transport. We need to model the influence of gravity on those sediments. Following Stokes' law, a sediment settlement velocity (or terminal velocity) depends on a characteristic sediment particle radius and its relative density to its carrier (eq. (25)).

$$\upsilon_i^{s_k} = \frac{2}{9} (r^{s_k})^2 \frac{\rho^{s_k} - \rho_0}{\mu} \mathbf{g}\, f(C_i^{s_k}) \tag{25}$$

Where υ^{s_k} denotes the settlement velocity for the sediment k, r^{s_k} the radius of a sediment k particle, and ρ^{s_k} the sediment k density. To prevent over-saturation due to advection, [WCMT07] uses the Richardson-Zaki relation $f(C^{s_k})$ [RZ54] which guarantees that the sediment concentration doesn't exceed its maximal level MaxC^{s_k}. This relations uses a control parameter $\kappa_{\mathrm{concentr}} \in [4; 5.5]$:

$$f(C^{s_k}) = \begin{cases} 1 - (C^{s_k}/\mathrm{MaxC}^{s_k})^{\kappa_{\mathrm{concentr}}} & , C^{s_k} < \mathrm{MaxC}^{s_k} \\ 0 & , C^{s_k} \geq \mathrm{MaxC}^{s_k} \end{cases} \tag{26}$$

The terminal velocity of a spherical particle falling in a steady fluid is given by (25). We use this formulation to express the velocity of sediments in fluids both external and inside the pores of the objects. As in Section 3.2, we propose another donor-acceptor scheme to solve sediment advection between particles with the following equation:

$$\mathrm{AdvV}_i^{s_k} = -\sum_j \begin{cases} V_j^f V_j^{s_k} \mathrm{filter}_{(i,j)} (\upsilon_{ij}^{s_k} \cdot \hat{\mathbf{x}_{ij}}) \nabla W_{ij} & , \upsilon_{ij}^{s_k} \cdot \mathbf{x}_{ij} \geq 0 \\ V_i^f V_i^{s_k} \mathrm{filter}_{(i,j)} (\upsilon_{ij}^{s_k} \cdot \hat{\mathbf{x}_{ij}}) \nabla W_{ij} & , \upsilon_{ij}^{s_k} \cdot \mathbf{x}_{ij} < 0 \end{cases} \tag{27}$$

Where $\upsilon_{ij}^{s_k}$ is the sediment velocity with the lowest norm between $\upsilon_i^{s_k}$ and $\upsilon_j^{s_k}$ to constrain the advected volume flow.

Any sediment present in the absence of water will be deposited. We explicitly control the deposition from fully-evaporated water particles by spreading the sediment volume to surrounding non-filled particles or spawning a new solid particle at the aforementioned fluid particle position (see Section 4.1).

3.4. Erosion

Erosion is an important process in weathering and has a substantial impact on the geometry of objects. It transforms cohesive materials into small particles by tearing them from the surface. In our simulation, it means the solid volume transforms into a sediment volume in the fluid phase. Fluid in contact with solid matter induces shear stress σ_{ij} caused by the relative velocity of the fluid to the solid surface. Since the interaction only happens between solid and fluid phases, we can ignore this process when i and j are in the same phase.

Figure 5: *Erosion, transport and deposition of a brittle material (brown) over an immutable material (white). Each row depicts a specific simulation step. From left to right: simulation result, sediments shown in green within the fluid, solid particles only.*

$$\sigma_{ij} = \left(\frac{\|\upsilon_i - \upsilon_j\|}{\|\mathbf{x}_{ij}\|} \right)^{0.5} \tag{28}$$

When σ_{ij} becomes greater than the intrinsic stress resistance of the material σ^k, erosion occurs.

Because erosion only occurs at the interface between solid and fluid, it is dependent on the contact area between the two phases. In our context, we consider this contact area as the area of the tangent face of the enclosing cube of our particle (i.e. $(2r)^2$ with r being the particle radius). We propose to compute the erosion rate of the material k for fluid particles i and solid particles j with the following equations:

$$\frac{\partial V_i^{s_k}}{\partial t} = (2r)^2 \kappa_{\mathrm{erosion}} \sum_j \begin{cases} \frac{V_j^k}{V_j} (\sigma_{ij} - \sigma^k), & \sigma_{ij} > \sigma^k \\ 0, & \sigma_{ij} \leq \sigma^k \end{cases} \tag{29}$$

$$\frac{\partial V_j^k}{\partial t} = -(2r)^2 \frac{V_j^k}{V_j} \kappa_{\mathrm{erosion}} \sum_i \begin{cases} (\sigma_{ij} - \sigma^k), & \sigma_{ij} > \sigma^k \\ 0, & \sigma_{ij} \leq \sigma^k \end{cases} \tag{30}$$

Where V^k is the volume of solid material k and $\kappa_{\mathrm{erosion}}$ is a control parameter. In practice, this formulation could result in an exchanged volume superior to the volume present in the solid particles. Indeed, in the case of strong shear stress or low volume particle, the computed values can get bigger than the actual volume of the particle. In such a case, we perform an explicit exchanged volume verification and clamp the results if necessary to guarantee volume conservation. The solid volume boundary handling is further discussed in Section 4.1.

3.5. Dissolution

Some granular materials have a stronger affinity to water molecules than their surrounding ones. This affinity is called solubility, and these materials are considered soluble (e.g., sugar, salts ...). The

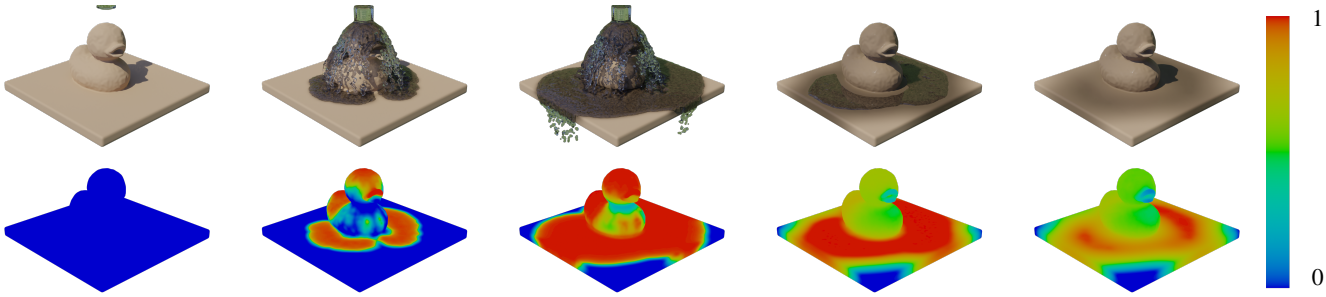

Figure 6: *Wetting and drying process of a porous material. Top: rendered view. Bottom: Heatmap of the pore saturation in water.*

capacity of a material to be dissolved by water is correlated to its capacity to diffuse within the water.

Unlike erosion, dissolution does not require forces such as shear stress to occur. This process only depends on the contact area between the two phases and the sediment concentration C^{s_k} in the fluid phase. We use a variation of equation (24) with a concentration set to MaxC^{s_k} for solid particles containing the material k. For a fluid particle i and solid particles j, dissolution can be written:

$$\frac{\partial V_i^{s_k}}{\partial t} = (2r)^2 \sum_j V_j^k D^{s_k} (C_i^{s_k} - C_j^{s_k}) \nabla^2 W_{ij} \tag{31}$$

$$\frac{\partial V_j^{s_k}}{\partial t} = (2r)^2 V_j^k \sum_i D^{s_k} (C_j^{s_k} - C_i^{s_k}) \nabla^2 W_{ij} \tag{32}$$

As the dissolution process can be altered by various external factors (such as temperature, pressure, acidity, basicity, etc.) and depends on the material considered, we rely on this simplified model where we neglect these factors. Accounting for these factors would be a clear venue for future works.

3.6. Evaporation

Evaporation is a phenomenon that occurs on the surface of a liquid that progressively changes it to gas (i.e., vaporization). It is a key component of the aging process as it contributes to sediment deposition and crystallization. Moreover, it guides water flow in the pore space by draining water from the surface, thus causing an internal flow to reach the surface. Evaporation is mainly influenced by two factors: Temperature and Relative Humidity.

Temperature diffusion is constrained by a temperature diffusivity α which is defined for each material. Temperature T variations is given by Fick's law of diffusion:

$$\frac{\partial T}{\partial t} = \alpha \nabla^2 T \tag{33}$$

For each particle, we compute α_i as a weighted average of its composing materials intrinsic heat diffusivity. The heat diffusivity of fluid particles is constant and set to water heat diffusivity (e.g. $\alpha_i \approx 0.143\text{e-}6\ \text{m}^2 \cdot \text{s}^{-1}$). We can compute the temperature diffusion using the SPH formalism:

$$\frac{\partial T_i}{\partial t} = -\sum_j min(\alpha_i, \alpha_j)(T_i - T_j) V_j \nabla^2 W_{ij} \tag{34}$$

Relative humidity is the proportion of *the amount of water vapor in the air* and *the water vapor the air would contain at a specific temperature to balance fluid surface evaporation*. This ratio can be interpreted as the propensity of the air to capture molecules from a fluid surface. The relative humidity H is defined as the ratio of partial water vapor pressure p^w and the equilibrium water vapor pressure p^{*w}.

In our case, H is set by the user as the input scene meteorological condition. In order to estimate the equilibrium water vapor pressure p^{*w} (eq. (35)), we use the Buck equation [Buc81] which exhibits the best accuracy between 0 and 100 degrees celsius. Most natural phenomena involving material transport matches this range.

$$p^{*w}(T) = 6.1121 \cdot e^{(18.678 - \frac{T}{234.5}) \cdot \frac{T}{257.14+T}} \tag{35}$$

Since we want to obtain the partial pressure of water vapor in the air p^w, using the known relative humidity H_{air} and temperature of the air T_{air}, we can compute:

$$p^w_{\text{air}} = H p^{*w}(T_{\text{air}}) \tag{36}$$

In our case, since we want to know the evaporation rate on our surface, we consider its partial water vapor pressure as its equilibrium state for a given temperature. The water vapor pressure at a surface particle i is then given by:

$$p_i^w = p^{*w}(T_i) \tag{37}$$

Pressure gradient is given by the difference between p^w_{air} and p_i^w. Taking into account the contact area between a particle and the air (see Section 3.4) and a control factor κ_{evap} (set to 10^{-3} in shown examples), we compute the evaporated or condensed amount of water as:

$$\frac{\partial V_i^f}{\partial t} = \kappa_{\text{evap}}\ (2r)^2 (p_i^w - p^w_{\text{air}}) \tag{38}$$

3.7. Sediment Deposition

We have seen how external water moves around the scene, how it interacts with porous mediums, and how it gets transported through the pore space. In addition, we have seen how sediments can form by being ripped off the surface of the solid or dissolved in the fluid and how the fluid transports those sediments. To finalize our sediment transport model, we need to account for the phase transition of the sediments from fluid-carried to solid. In this section, we

study volume transfer from the fluid phase to the solid phase from a physical perspective. Stable solid particle insertion and volume evolution of the surface are addressed in Section 4.1.

The deposition is the result of particles settling on a solid surface. When sediments are denser than water or when concentration is above water capacity, deposition will occur. This process is responsible for the transformation of sediment into solid matter.

As previously studied in Section 3.3, sediments settle in a fluid following equation (27). We modify this formulation for surface interaction between a fluid particle i and a surface solid particle j:

$$\frac{\partial V_j^k}{\partial t} = (2r)^2 \sum_i \kappa_{\text{depos}} V_i^{s_k} (\upsilon_{ij}^{s_k} \cdot \hat{\mathbf{x}_{ij}}) \nabla W_{ij} \tag{39}$$

Where κ_{depos} is a control parameter affecting the amount of deposition. In addition, when a fluid particle become overly concentrated ($C_i^{s_k} > \text{MaxC}^{s_k}$) due to volume loss (e.g. evaporation and penetration in porous medium), sediments must be deposited on a nearby existing surface. In this case, we transfer the excess sediment volume in the fluid particle to nearby surface solid particles.

4. Implementation Details

In the simulation, spawning and deleting particles is a delicate process that must be carefully implemented to ensure stability. Due to the multiple phenomena our method handles, particles must appear and disappear to best represent the weathering scene. In our simulations, particles can only appear and disappear near the phases boundary. To enforce stability, we must ensure the boundary does not show abrupt changes over time. In this section, we describe how to handle volume variation at the boundary and how to handle outflow from a porous material.

4.1. Solid Volume Variation

In weathering, multiple important phenomena are related to interactions between different phases. A key aspect of our method is the handling of boundaries and their evolution over time. Due to deposition, dissolution, and erosion, material volumes can switch from one phase to another. When this happens, it creates a volume variation in the solid phase. We thus have to take into account the boundary modification accordingly.

If we only consider the solid volume scalar field for each particle during the external flow process, fluid particles could slip through solids to compensate for the volume loss of the solid particles. To ensure the iso-surface remains continuous, we adapted the boundary model defined by Akinci et al. [AIA*12] which overestimates the density of particles at the boundary of the solid. In our case, we account for the solid volume variation at boundary as:

$$\text{BoundaryVolume}(i) = \frac{V_i}{\sum_j V_j W_{ij}} \tag{40}$$

Weathering effects such as dissolution and erosion will remove matter from the material, whereas deposition will add matter onto the surface. These effects hence compete against each other. If managed sequentially, the result of those phenomenons would be order-dependent and would require multiple neighborhood recomputation. On the other hand, performing all operations at once before applying them to the simulation allows us to break the order-dependency and reduce the overall cost of a simulation step. Up to this point, we know the amount of matter variation at the boundary, and we need to reflect it on the solid boundary.

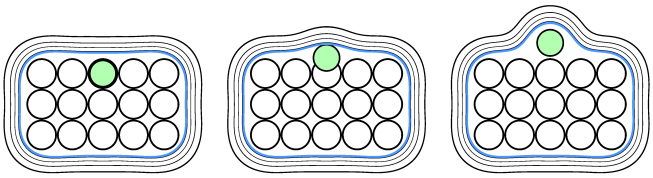

Figure 7: *When solid sediment are deposited on another surface a new particle must be created (shown in green) to account for the volume change. As its volume ratio (eq. (40)) increases through time (from left to right: 0.0, 0.5, 1.0), the novel particle is gradually displaced to its final grid position.*

In practice, we chose to organize solid materials using a regular grid to ensure solid particles are evenly spaced within the material, preventing discontinuities. In addition, this regular grid facilitates the detection of boundary solid particles. For each grid cell, we associate at most a single solid particle. The grid cell position represents the particle position when it reaches the maximum particle volume (restricted by the kernel radius). The particle position $\mathbf{x}_i$ at the boundary of the solid can be obtained by doing a linear interpolation between the associated grid cell position $\mathbf{x}_i^{\text{grid}}$ and a target position below the surface $\mathbf{x}_i^{subsurface}$ using its volume ratio V_i/V_{max}. This target position is given by:

$$x_i^{subsurface} = \mathbf{x}_i^{\text{grid}} - 2r \frac{\hat{\mathbf{N}}}{\max(|n_x|, |n_y|, |n_z|)} \tag{41}$$

Where $\hat{\mathbf{N}}$ is the normalized normal vector $\mathbf{N} = (n_x, n_y, n_z)^t$ obtained by evaluating the density field gradient at $\mathbf{x}_i$. Then, when a particle loses volume, its position moves toward the interior of the solid material. When its volume reaches zero, the particle is fully merged in the surface. Thus, simply removing the particle from the simulation does not introduce any discontinuities. Similarly, when matter is added to the surface, new particles are spawned at the boundary and shifted toward the object's interior. As their volume increase, the newly-created particles progressively reach their final position without creating discontinuities on the surface (as seen in Fig. 7).

4.2. Fluid Outflow

As previously discussed in Section 3.2, water can travel through the pore space of a solid material. The water volume exchanged between particles is described using equations (15) and (17). Since fluid particles are considered saturated, and diffusion transfers fluid volume from saturated particles to lesser ones, diffusion will not cause outward flow.

Using equation (17), water volume is transferred from a solid

volume particle to a fluid particle j if and only if it is located toward the advection direction ($\rho_0 \mathbf{g} \cdot \mathbf{x}_{ij} > 0$) and $V_j^f < V_{max}$. New fluid particles are spawned near the surface when the porous material contains water, and there are no fluid particles near the surface.

5. Results

In this section, we explicit the process of turning the resulting simulated data into exploitable assets for a standard renderer workflow, as well as discuss the results shown in our paper.

Rendering: Figures shown in this paper are rendered using the following pipeline. For each phase (fluid and solid), we project the density field using SPH continuum equation (see eq. (1)) on a 3D lattice vertices. It allows us to reconstruct the surface of each phase by using a marching cube algorithm. To represent the sediments contained within the fluid phase, we export a concentration field for each by sampling their volume scalar field at each voxel of a sparse grid using OpenVDB format. Those fields will later be used as the absorption parameters of a volume BSDF.

Because we chose to use a physically-based rendering (PBR) workflow, material textures (albedo, metallic, roughness, specular) are created for the solid surface. We create a UV-parametrization of the surface, and for each texel of the PBR texture, we sample the material volume scalar fields accordingly and perform a weighted average of the material parameters. In addition, the albedo is modified to account for the presence of sediments within the object pores. This is obtained by using the porosity scalar field and a per-sediment absorption parameter. The wetting effect is achieved by darkening the material and increasing its clearcoat. Alternatively, approaches like [HPMG06, BDP21] can be used to render wet porous materials. Finally, these data are fed into a standard production rendering engine (e.g. Blender) to produce realistic imagery.

Note that this specific rendering pipeline is purely illustrative, and some of the chosen effects are exaggerated for better readability.

Results: Our approach can model the interaction of multiple phenomena, leading to a weathered representation of a 3D scene. In this section, we describe how different combinations of elementary phenomena can create different effects on the scene.

First, In Figures 1 and 4 we demonstrate a simple example of the capability of our framework. In this example, we simulate making coffee as in any good morning routine. This simulation combines three distinct elementary phenomena to recreate the wanted effect. First, the water is poured onto the dry coffee, then, the coffee ***dissolves*** into the water, and finally the water ***transport*** the coffee sediment across the filter through ***porous flow*** and drips into the glass.

Then, in figure 5, we demonstrate erosion, sediment transport, and deposition in a simple scene where a fluid is poured on brittle material similar to sand. In this example, the brittle material is ***eroded*** and captured by the fluid as sediment and then ***transported*** within the fluid. Finally, the sediments are ***deposited*** elsewhere in the scene.

In figure 6, we show a simulation that illustrates the porous flow and evaporation. This scene is composed of single highly porous material that gets "wetted" by flow spray. This simulation shows how the ***porous flow*** helps transport fluid across a material. Finally, the fluid ***evaporates***, and the material slowly goes back to its initial state. This simulation also illustrates the importance of simulating as many elementary phenomena as possible, especially those that modify the object boundary and composition.

Figure 8: *Stains produced by dirty water coming out of a hole. It shows diffusion of water and sediments in the medium and deposition on the surface after evaporation.*

In figure 8, we simulate pouring saturated fluid onto a slightly porous material. In this simulation, the fluid is saturated with colored sediment. These sediments are ***transported*** by the water through the ***porous flow***, and leave colored stains when the fluid ***evaporates***.

Figure 9 is the summarization of the different effects illustrated previously. Water is poured over a volume of soil, ***eroding*** it as it flows and carrying sediments over two materials, one waterproof and a porous one. Leaving ***deposits*** on the impervious surface and ***stains*** on the porous wall. Finally, the saturated water ***penetrates*** the wall and ***seeps*** into the base of the wall.

Finally, in figure 10, we simulate the complex process of efflorescence formation. This process happens when salt sediments (gypsum) are deposited when fluid (groundwater) ***transports*** it through a material ***porous space*** via capillary action. These sediments are ***deposited*** on the surface of the object due to the ***evaporation*** of their carrier fluid.

6. Discussion & Limitations

As shown above, our method can handle interactions between the pore space and external fluids. However, it does not account for in-

teractions within the pore space. For instance, when fluid travels in the porous medium, dissolution can affect the size of internal pores. Similarly, sediment deposition or crystallization can also affect the internal geometry of the object and can lead to internal stress or structure deformations (e.g., cracks caused by salt crystallization, peeling paint layer on a wet wood surface). Considering these internal interactions would be a promising venue for future works.

Since wetting plays an essential role in a wide range of phenomena, it would be interesting to study the airflow and its interaction with the porous medium. It would allow a more accurate model of the water vapor pressure in the whole volume instead of relying solely on the temperature at the interface. Furthermore, a refined water vapor model could allow for a precise organic growth model within the porous mediums. In a more general manner, chemical interactions between fluid, sediments and solid matter could widen the range of phenomena we can depict (e.g. rust formation, corrosion) and enrich our simplified dissolution model.

In the case of water flowing through and dripping from a material (as illustrated in Fig. 1 and Fig. 4), the fluid outflow described in Section 4.2 requires the creation of new particles. As newly created particles may have a low volume, the number of particles considered within the neighborhood can be large, hampering performances in the scenes mentioned earlier.

All results shown in this work consider solid volumes to be static. In order to integrate moving objects, approaches relying on per-object local grids (like [WCMT07]) could be considered. However, our proposed solid volume handling (see Section 4.1) should be unsuitable in the context of multiple moving objects. More specially, objects that are close to each other must be carefully considered when new particles spawn at their common interface and should require taking to account mechanical forces. Despite everything, our proposed porous flow model should remain correct if we integrate motion acceleration during advection computations.

7. Conclusion & Future Works

Our main objective is to produce the weathered representation of a pristine scene to enrich realistic imagery. In this context, we presented a framework based on SPH to model interactions between porous objects, fluid, and sediments.

This model can depict reversible phenomena like wetting and evaporation. It can also handle alteration of the object geometry through dissolution, deposition, and erosion and the alteration of object appearance via deposition and sediment transport. Through the interactions between these processes, our framework successfully approximates physically plausible results which can be found in nature.

More interactions between materials could be accounted for in future works by solving the chemical reactions occurring in the scene. Furthermore, the accurate simulation of interactions within the pore space could lead to new research in organic growth and mechanical simulation for weathering. Finally, using the simulation data to deduce a mesoscale spatially-varying BSDF could reduce the gap between simulations of the aging process and the rendering of a weathered scene.

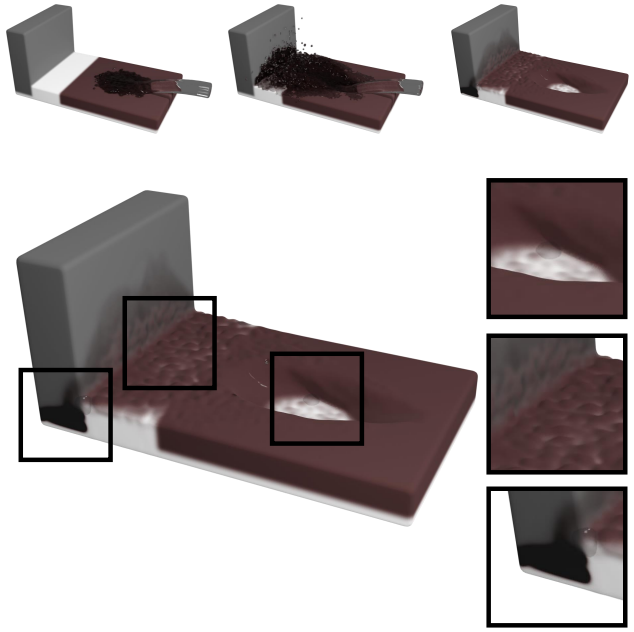

Figure 9: *Erosion, Transport, Deposition and Porous flow occurring in the same scenario.* ***Top row*** *shows differents points of the animation: before, during and after the water jet.* ***Middle*** *exhibits the outcome of the simulation.* ***Insets*** *depicts close-ups of the illustrated effects, from top to bottom: erosion, deposits and stains, porous flow.*

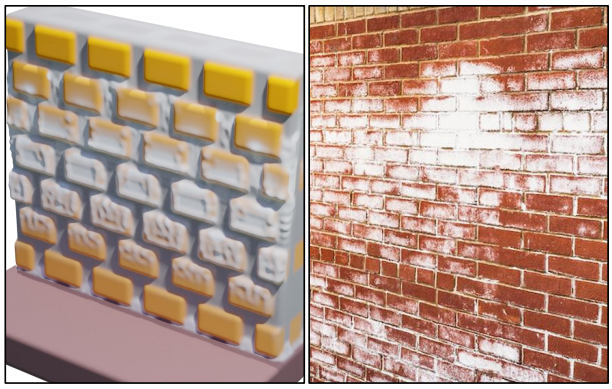

Figure 10: *Efflorescence process on a brick wall. Salt is carried from the underground to the surface by ground water. It then deposits on the surface due to evaporation resulting in gypsum formation.* ***Top row****: Pristine wall.* ***Bottom row****: Weathered wall.* ***Left column****: Particle representation.* ***Right column****: Rendered result.*

Acknowledgements

This research work acknowledges support from project HDWorlds from the Agence Nationale de la Recherche (ANR-16-CE33-0001).

References

[AAT13] AKINCI N., AKINCI G., TESCHNER M.: Versatile surface tension and adhesion for sph fluids. *ACM Trans. Graph. 32*, 6 (Nov. 2013). URL: https://doi.org/10.1145/2508363.2508395, doi:10.1145/2508363.2508395. 5

[AIA*12] AKINCI N., IHMSEN M., AKINCI G., SOLENTHALER B., TESCHNER M.: Versatile rigid-fluid coupling for incompressible sph. *ACM Trans. Graph. 31*, 4 (July 2012). URL: https://doi.org/10.1145/2185520.2185558, doi:10.1145/2185520.2185558. 9

[BB90] BECKET W., BADLER N. I.: Imperfection for realistic image synthesis. *The Journal of Visualization and Computer Animation 1*, 1 (1990), 26–32. URL: https://onlinelibrary.wiley.com/doi/abs/10.1002/vis.4340010108, arXiv:https://onlinelibrary.wiley.com/doi/pdf/10.1002/vis.4340010108, doi:https://doi.org/10.1002/vis.4340010108. 1

[BDP21] BAJO J. M., DELRIEUX C., PATOW G.: Physically inspired technique for modeling wet absorbent materials. *The Visual Computer 37*, 8 (2021), 2053–2068. 10

[BKCO16] BELLINI R., KLEIMAN Y., COHEN-OR D.: Time-varying weathering in texture space. *ACM Trans. Graph. 35*, 4 (July 2016). URL: https://doi.org/10.1145/2897824.2925891, doi:10.1145/2897824.2925891. 3

[BLR*11] BOSCH C., LAFFONT P.-Y., RUSHMEIER H., DORSEY J., DRETTAKIS G.: Image-guided weathering: A new approach applied to flow phenomena. *ACM Trans. Graph. 30*, 3 (May 2011). URL: https://doi.org/10.1145/1966394.1966399, doi:10.1145/1966394.1966399. 3

[Buc81] BUCK A. L.: New equations for computing vapor pressure and enhancement factor. *Journal of Applied Meteorology and Climatology 20*, 12 (1981), 1527 – 1532. URL: https://journals.ametsoc.org/view/journals/apme/20/12/1520-0450_1981_020_1527_nefcvp_2_0_co_2.xml, doi:10.1175/1520-0450(1981)020<1527:NEFCVP>2.0.CO;2. 8

[BW09] BANDEIRA D., WALTER M.: Synthesis and transfer of time-variant material appearance on images. pp. 32–39. doi:10.1109/SIBGRAPI.2009.38. 3

[CXW*05] CHEN Y., XIA L., WONG T.-T., TONG X., BAO H., GUO B., SHUM H.-Y.: Visual simulation of weathering by gamma-ton tracing. In *ACM SIGGRAPH 2005 Papers* (New York, NY, USA, 2005), SIGGRAPH '05, Association for Computing Machinery, p. 1127–1133. URL: https://doi.org/10.1145/1186822.1073321, doi:10.1145/1186822.1073321. 3

[Dar56] DARCY H.: *Les fontaines publiques de la ville de Dijon: exposition et application...* Victor Dalmont, 1856. 5

[DEJ*99] DORSEY J., EDELMAN A., JENSEN H. W., LEGAKIS J., PEDERSEN H. K.: Modeling and rendering of weathered stone. In *Proceedings of the 26th Annual Conference on Computer Graphics and Interactive Techniques* (USA, 1999), SIGGRAPH '99, ACM Press/Addison-Wesley Publishing Co., p. 225–234. URL: https://doi.org/10.1145/311535.311560, doi:10.1145/311535.311560. 3, 5

[DH96] DORSEY J., HANRAHAN P.: Modeling and rendering of metallic patinas. In *Proceedings of the 23rd Annual Conference on Computer Graphics and Interactive Techniques* (New York, NY, USA, 1996), SIGGRAPH '96, Association for Computing Machinery, p. 387–396. URL: https://doi.org/10.1145/237170.237278, doi:10.1145/237170.237278. 3

[DPH96] DORSEY J., PEDERSEN H., HANRAHAN P.: Flow and changes in appearance. *Proc. SIGGRAPH 96* (08 1996), 3. doi:10.1145/1198555.1198696. 3

[DRS07] DORSEY J., RUSHMEIER H., SILLION F. X.: *Digital Modeling of Material Appearance*. Computer Graphics. Morgan Kaufmann / Elsevier, Dec. 2007. URL: https://hal.inria.fr/inria-00510244. 1

[GPH*18] GAO M., PRADHANA A., HAN X., GUO Q., KOT G., SIFAKIS E., JIANG C.: Animating fluid sediment mixture in particle-laden flows. *ACM Transactions on Graphics (TOG) 37*, 4 (2018), 1–11. 3

[HPMG06] HNAT K., PORQUET D., MERILLOU S., GHAZANFARPOUR D.: Real-time wetting of porous media. *MG&V 15*, 3 (Jan. 2006), 401–413. 10

[HPS11] HUBER M., PABST S., STRASSER W.: Wet cloth simulation. In *ACM SIGGRAPH 2011 Posters*. 2011, pp. 1–1. 3

[KBKS09] KRISTOF P., BENES B., KRIVANEK J., STAVA O.: Hydraulic erosion using smoothed particle hydrodynamics. *Computer Graphics Forum 28* (04 2009), 219 – 228. doi:10.1111/j.1467-8659.2009.01361.x. 3, 6

[KBST19] KOSCHIER D., BENDER J., SOLENTHALER B., TESCHNER M.: Smoothed particle hydrodynamics techniques for the physics based simulation of fluids and solids. doi:10.2312/egt.20191035. 4, 5

[LAD08] LENAERTS T., ADAMS B., DUTRÉ P.: Porous flow in particle-based fluid simulations. *ACM Trans. Graph. 27*, 3 (Aug. 2008), 1–8. URL: https://doi.org/10.1145/1360612.1360648, doi:10.1145/1360612.1360648. 3, 5

[LDR09] LU J., DORSEY J., RUSHMEIER H.: Dominant texture and diffusion distance manifolds. *Computer Graphics Forum 28*, 2 (2009), 667–676. URL: https://onlinelibrary.wiley.com/doi/abs/10.1111/j.1467-8659.2009.01407.x, arXiv:https://onlinelibrary.wiley.com/doi/pdf/10.1111/j.1467-8659.2009.01407.x, doi:https://doi.org/10.1111/j.1467-8659.2009.01407.x. 3

[LGG*07] LU J., GEORGHIADES A. S., GLASER A., WU H., WEI L.-Y., GUO B., DORSEY J., RUSHMEIER H.: Context-aware textures. *ACM Trans. Graph. 26*, 1 (Jan. 2007), 3–es. URL: https://doi.org/10.1145/1189762.1189765, doi:10.1145/1189762.1189765. 3

[MG08] MÉRILLOU S., GHAZANFARPOUR D.: A survey of aging and weathering phenomena in computer graphics. *Computers & Graphics 32*, 2 (2008), 159 – 174. URL: http://www.sciencedirect.com/science/article/pii/S0097849308000058, doi:https://doi.org/10.1016/j.cag.2008.01.003. 1

[MKC*06] MERTENS T., KAUTZ J., CHEN J., BEKAERT P., DURAND F.: Texture Transfer Using Geometry Correlation. In *Symposium on Rendering* (2006), Akenine-Moeller T., Heidrich W., (Eds.), The Eurographics Association. doi:10.2312/EGWR/EGSR06/273-284. 3

[MMGG12] MÉRILLOU N., MERILLOU S., GALIN E., GHAZANFARPOUR D.: Simulating how salt decay ages buildings. *IEEE Computer Graphics and Applications 32* (03 2012), 44–54. doi:10.1109/MCG.2011.107. 3

[Mon05] MONAGHAN J.: Smoothed particle hydrodynamics. *Reports on Progress in Physics 68* (07 2005), 1703. doi:10.1088/0034-4885/68/8/R01. 5

[MPBM*18] MUÑOZ PANDIELLA I., BOSCH C., MERILLOU S., MÉRILLOU N., PATOW G., PUEYO X.: Urban weathering: Interactive rendering of polluted cities. *IEEE Transactions on Visualization and Computer Graphics PP* (01 2018), 1–1. doi:10.1109/TVCG.2018.2794526. 3

[MSKG05] MÜLLER M., SOLENTHALER B., KEISER R., GROSS M.: Particle-based fluid-fluid interaction. In *Proceedings of the 2005 ACM*

SIGGRAPH/Eurographics Symposium on Computer Animation (New York, NY, USA, 2005), SCA '05, Association for Computing Machinery, p. 237–244. URL: https://doi.org/10.1145/1073368.1073402, doi:10.1145/1073368.1073402. 6

[PC13] PATKAR S., CHAUDHURI P.: Wetting of porous solids. *IEEE transactions on visualization and computer graphics 19*, 9 (2013), 1592–1604. 3

[PPD02] PAQUETTE E., POULIN P., DRETTAKIS G.: The Simulation of Paint Cracking and Peeling. In *Proceedings of Graphics Interface* (Calgary, Canada, May 2002), Stuerzlinger W., McCool M., (Eds.), Canadian Human-Computer Communications Society, p. 10. URL: https://hal.inria.fr/inria-00606725. 3

[RKN12] RUNGJIRATANANON W., KANAMORI Y., NISHITA T.: Wetting effects in hair simulation. In *Computer Graphics Forum* (2012), vol. 31, Wiley Online Library, pp. 1993–2002. 3

[RSKN08] RUNGJIRATANANON W., SZEGO Z., KANAMORI Y., NISHITA T.: Real-time animation of sand-water interaction. In *Computer Graphics Forum* (2008), vol. 27, Wiley Online Library, pp. 1887–1893. 3

[RZ54] RICHARDSON J., ZAKI W.: Sedimentation and fluidisation. *Transactions of the Institution of Chemical Engineers 32* (1954), 35–53. URL: https://ci.nii.ac.jp/naid/10018486787/. 7

[SP09] SOLENTHALER B., PAJAROLA R.: Predictive-corrective incompressible sph. In *ACM SIGGRAPH 2009 Papers* (New York, NY, USA, 2009), SIGGRAPH '09, Association for Computing Machinery. URL: https://doi.org/10.1145/1576246.1531346, doi:10.1145/1576246.1531346. 5

[WCMT07] WOJTAN C., CARLSON M., MUCHA P. J., TURK G.: Animating corrosion and erosion. In *NPH* (2007), Citeseer, pp. 15–22. 3, 7, 11

[WTL*06] WANG J., TONG X., LIN S., PAN M., WANG C., BAO H., GUO B., SHUM H.-Y.: Appearance manifolds for modeling time-variant appearance of materials. In *ACM SIGGRAPH 2006 Papers* (New York, NY, USA, 2006), SIGGRAPH '06, Association for Computing Machinery, p. 754–761. URL: https://doi.org/10.1145/1179352.1141951, doi:10.1145/1179352.1141951. 2

[XWT*08] XUE S., WANG J., TONG X., DAI Q., GUO B.: Image-based material weathering. *Computer Graphics Forum 27* (04 2008), 617 – 626. doi:10.1111/j.1467-8659.2008.01159.x. 3